ACS OMEGA

Open Access

http://pubs.acs.org/journal/acsodf

Article

Curcumin-Encapsulated Co-ZIF-8 for Ulcerative Colitis Therapy: ROS Scavenging and Macrophage Modulation Effects

Qi Tao, Hang Yao,* Feifei Wang, Zehao Gu, Xiaofei Yang, Yuchi Zhao, Huan Pang, Dong-An Wang,* and Hui Chong*

Cite This: *ACS Omega* 2024, 9, 30571−30582

Read Online

ACCESS | Metrics & More | Article Recommendations | Supporting Information

ABSTRACT: Ulcerative colitis (UC) is a chronic inflammatory bowel disease characterized by the disruption of the intestinal epithelial barrier. This study described the synthesis and characterization of CCM-Co-ZIF-8, a novel composite material with enzyme-like activities similar to catalase, peroxidase, and superoxide dismutase. CCM-Co-ZIF-8 demonstrated the ability to scavenge reactive oxygen species that play a critical role in UC pathogenesis. In vitro studies using lipopolysaccharide-induced RAW264.7 cells showed that CCM-Co-ZIF-8 exhibited anti-inflammatory activity by promoting the transition of macrophages from an M1 to an M2 phenotype. In vivo experiments using a mouse model of UC demonstrated that CCM-Co-ZIF-8 suppressed the expression of proinflammatory cytokines. These findings suggested that CCM-Co-ZIF-8 might hold promise as a therapeutic strategy for the treatment of UC.

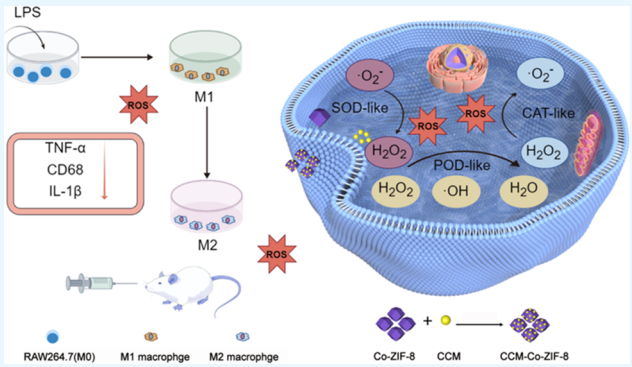

1. INTRODUCTION

Inflammatory bowel disease (IBD) is a chronic and relapsing pathema characterized by intestinal ulcers and damage to the epithelial barrier.[1] Ulcerative colitis (UC) is a common form of IBD that specifically affects the colon, primarily involving the mucosal and submucosal layers, and often manifests in adolescence.[2,3] The therapeutic modalities for UC include pharmacological interventions and emerging biologic therapies.[4] Pharmacological treatment mainly involves the use of corticosteroids, aminosalicylates, and immunosuppressants.[5,6] However, excessive medication may entail possible adverse reactions and the possibility of an unsuccessful efficacy. Therefore, there is an urgent need for suitable therapeutic strategies for UC. The development of UC encompasses various processes, including inflammation, compromised epithelial barrier integrity, and oxidative harm.[7] In the early stages of UC, macrophages, dendritic cells, and other antigenic presenting cells initiate a series of proinflammatory and anti-inflammatory signals that cause immune cells to migrate to the site of inflammation, and these immune cells penetrate the mucosa.[8] Deficiencies in the mucin barrier provoke possible immune dysregulation and consequent inflammation within the intestines.[9] Aberrant demise of intestinal epithelial cells (IECs) can escalate the inflammatory reaction and trigger injury to the intestinal mucosa.[10,11] Reactive oxygen species (ROS) constitute a significant class of highly reactive oxygen-containing chemicals that can originate from either exogenous or endogenous sources.[12] Impaired antioxidant capacity leading to excess ROS is a critical factor in oxidative damage. In inflammatory bowel disease, infiltrating neutrophils generate a substantial amount of ROS. Excessive ROS acting on endothelial cells lead to oxidative damage, exacerbating the inflammatory process.[13]

Eliminating excess ROS is crucial for addressing oxidative injury. Wang et al. synthesized hyaluronic acid-guided cerium dioxide nanoenzymes that are compatible and stable, showing an increased superoxide dismutase-like activity with increasing Ce(III)/Ce(IV) ratio that could effectively eliminate ROS. These nanoenzymes also have potential therapeutic effects on atherosclerosis.[14] Additionally, the modulation of macrophages during the inflammatory stage assumes a vital significance in the management of UC.[15] Macrophages exhibit two phenotypic forms in vivo: M1 for proinflammatory and M2 for anti-inflammatory. Macrophages of the M1 subtype release copious quantities of proinflammatory cytokines, notably including interleukin 1β (IL-1β).[16,17] Correspondingly, M2 macrophages can impede the advancement of inflammation by releasing substances that have anti-inflammatory effects, such as interleukin-4 (IL-4).[18,19] Imbalance in polarization between

Received: March 13, 2024
Revised: June 11, 2024
Accepted: June 18, 2024
Published: July 4, 2024

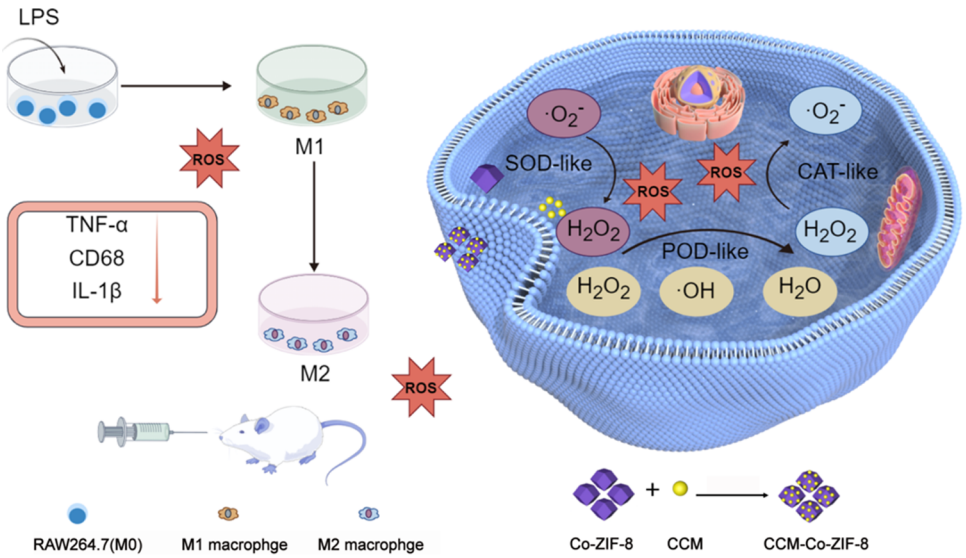

Figure 1. Proposed mechanism for the treatment of ulcerative colitis by CCM-Co-ZIF-8.

the M1 and M2 macrophages can exacerbate the inflammatory process. Studies have reported that Prussian blue analogs loaded with curcumin (CCM) possess the ability to convert M1 macrophages into the M2 phenotype, demonstrating the significant potential of curcumin in macrophage polarization.[20]

Metal−organic frameworks (MOFs) offer well-defined pores and channels, thus providing hydrophobic coordination environments similar to natural enzymes.[21] In addition, MOFs demonstrate inherent enzyme-mimicking properties, making them suitable candidates for synthetic enzymes. Transition metals such as iron, cobalt, and copper serve as typical metal centers for the preparation of catalytically active MOFs. Sang et al. discovered that cobalt-based MOFs (ZIF-67), constructed by Co^{2+} and dimethylimidazole, exhibit outstanding nanozyme activity.[22] Yang et al. reported the synthesis of Co-MOF under hydrothermal conditions, which demonstrated inherent peroxidase-like activity.[23] Among the reported MOFs, ZIF-8 is a zeolitic imidazolate framework synthesized through coordination between zinc nitrate and 2-methylimidazole molecules. Its geometric structure bears a resemblance to the active site of human carbonic anhydrase II and exhibits excellent catalytic performance. When these zinc cations interact with water molecules, the pK_a value of water significantly decreases from 14 to 8.4, favoring the deprotonation process of water. This phenomenon generates zinc-bound hydroxide nucleophilic reagents, which might enable catalysis of multiple biochemistry reactions.[24]

Conditioned culture medium (CCM) can modulate M1/M2 macrophage polarization, activate Toll-like receptor (TLR) signaling pathways, and elicit pharmacological effects including antioxidative, anticancer, and anti-inflammatory activities.[25,26] We engineered a novel composite material, termed CCM-Co-ZIF-8, by modifying the anti-inflammatory drug CCM and encapsulating it within Co-ZIF-8. Our goal for this study was to achieve a synergistic nanozyme effect and anti-inflammatory outcome. After convincing of the biocompatibility of CCM-Co-ZIF-8, we further tested the in vitro and in vivo anti-inflammatory effects together with the mechanisms (Figure 1). The results showed that CCM-Co-ZIF-8 displayed reactive oxygen species (ROS)-related nanozyme activities and could achieve macrophage subtype transformation (M1 to M2). Furthermore, the application of CCM-Co-ZIF-8 resulted in reduced symptoms in the UC mice model. We wish that the current material could be potentially used as a material for the treatment of UC. For patients with UC, it plays a dual regulatory role in clearing reactive oxygen species and alleviating inflammation.

2. MATERIALS AND INSTRUMENTS

2.1. Materials and Instruments. Chemicals for Co-ZIF-8 synthesis, acetic acid, hydrochloric acid, and 30% hydrogen peroxide were provided by Sinopharm Chemical Reagent Co., Ltd. LPS and anhydrous ethanol were supplied by Aladdin (Shanghai, China). TMB (3,3,5-tetramethylbenzidine) was purchased from Shanghai Jinsui Biological Technology Co., Ltd. Riboflavin, L-tryptophan, nitroblue tetrazolium chloride, and curcumin were procured from Sangon Biotech (Shanghai, China). DMEM medium, fetal bovine serum, 0.25% trypsin, penicillin−streptomycin (PS), and sodium pyruvate were obtained from Gibco. IL-4 and interleukin-13 (IL-13) were provided by Peprotech. Cell lysis reagent (Trizol) was purchased from Sigma-Aldrich. The PCR reverse transcription kit was obtained from Novozymes (Nanjing, Jiangsu). Freezing embedding medium was supplied by Leica.

2.2. Synthesis of Co-ZIF-8 and CCM-Co-ZIF-8. A 1.161 g amount of 2-methylimidazole was dissolved in a mixture of 10 mL of DMF (*N*,*N*-dimethylformamide) and methanol (DMF/methanol = 4:1). Simultaneously, 0.535 g of $Zn(NO_3)_2{\cdot}6H_2O$ and 0.535 g of $Co(NO_3)_2{\cdot}6H_2O$ were dissolved in another mixture of 15 mL of DMF and methanol (DMF/methanol = 4:1). Once fully dissolved, the solution containing 2-methylimidazole was added gradually drop by drop into the $Zn(NO_3)_2{\cdot}6H_2O$ and $Co(NO_3)_2{\cdot}6H_2O$ solutions while stirring at a speed of 700 rpm for a duration of 12 h. After centrifugation to remove the supernatant, the residue was washed repeatedly with methanol and the supernatant was discarded, each performed three times. After the excess liquid was removed, the obtained Co-ZIF-8 sample was air-dried at room temperature.

2.3. Material Characterization of Nanoparticles. Fourier transform infrared spectroscopy (FTIR) was performed using a Cary 610/670 instrument (Varian, USA) to determine

https://doi.org/10.1021/acsomega.4c02446
ACS Omega 2024, 9, 30571−30582

infrared spectra, analyze functional groups, and investigate potential intermolecular forces. Scanning electron microscopy (SEM) and transmission electron microscopy (TEM) were conducted using a Zeiss_Supra55 (Carl Zeiss, Germany) and JEM-2100 (JEOL, Japan), respectively. Nano Measurer software was employed for nanoparticle size analysis. X-ray diffraction (XRD) analysis was carried out by using a D8 Advance X-ray diffractometer (Bruker, Germany).

2.4. Assessment of SOD-like Enzyme Activity. The SOD-like activity of Co-ZIF-8 was evaluated by measuring the inhibition of NBT (nitroblue tetrazolium) photoreduction. Riboflavin (1.2 mM), methionine (0.13 M), NBT (1 mg/mL), EDTA·Na_2 (0.1 M), and different concentrations of Co-ZIF-8 (10, 15, 20, 40, 80, and 100 μg/mL) were sequentially added to PBS (pH = 7.40). The mixture was then exposed to an LED light for 15 min. After light exposure, the absorbance at 560 nm was immediately measured.

2.5. Assessment of CAT-like Enzyme Activity. The CAT-like activity of Co-ZIF-8 was assessed by measuring the dissolved oxygen concentration using a dissolved oxygen meter with a specialized oxygen electrode at room temperature. Kinetic analysis was conducted at room temperature using a 2 mL reaction buffer solution and a 2 mL Co-ZIF-8 solution. 2 mL of various concentrations of hydrogen peroxide (ranging from (4 to 2) $\times 10^{-3}$ M) were added to the reaction system containing Co-ZIF-8 (2 mL, 80 μg/mL). The dissolved oxygen concentration was monitored using the dissolved oxygen meter within 10 min. Different concentrations of Co-ZIF-8 solution (ranging from (0.12 to 2) $\times 10^{-3}$ mg/mL) were added to the reaction system containing hydrogen peroxide (2 mL, 4 M). The dissolved oxygen concentration was monitored using the dissolved oxygen meter within 400 s. All Michaelis−Menten constants were calculated based on the Michaelis−Menten saturation curves using Origin software.

2.6. Assessment of POD-like Enzyme Activity. A 2.80 mL reaction buffer solution (0.1 M NaAc, pH = 4.0) and 20 μL Co-ZIF-8 solution (final concentration of 50 μg/mL) were prepared at room temperature. 50 μL of 0.12 M TMB and 100 μL of different concentrations of hydrogen peroxide (ranging from 0.3 to 60 mM) were added to the reaction system containing Co-ZIF-8. The absorbance at 625 nm was recorded over time.

2.7. Drug Loading Performance of Co-ZIF-8. 3 mg portion of dried CCM-Co-ZIF-8 was dissolved in 50 μL of hydrochloric acid, followed by dilution with anhydrous ethanol to a final volume of 2 mL. UV−visible spectroscopy analysis was conducted at a wavelength of 425 nm; the drug loading efficiency and encapsulation efficiency were determined by utilizing a standard curve and calculating them using the formulas provided below

$$\text{drug loading efficiency (\%)} = \frac{\text{drug content on particles}}{\text{total weight of particles}} \times 100\%$$

$$\text{encapsulation efficiency (\%)} = \frac{\text{loaded drug amount}}{\text{total feeded drug amount}} \times 100\%$$

A 2 mg portion of CCM-Co-ZIF-8 was dissolved in a mixture of 20 mL of PBS and Tween-20 solution (pH = 5.0), followed by continuous shaking at 37 °C and 120 rpm. At selected time intervals (0, 1, 2, 3, 5, 18, 36, 48, 60 h), 1 mL of the solution was centrifuged and redispersed with 1 mL of PBS solution. The release of curcumin was measured at a wavelength of 425 nm by using UV−visible spectroscopy, and the obtained values were correlated with a calibration curve. The cumulative release percentage was calculated within the selected time intervals.

2.8. Cytotoxicity of Co-ZIF-8 and CCM-Co-ZIF-8. RAW264.7 and human epithelial cells (L929, ATCC) were cultured in GIBCO media supplemented with 10% fetal bovine serum for 24 h. The effects of different concentrations (3, 5, and 8 μmol/L) of pure curcumin, 1, 5, and 10 mg/L of Co-ZIF-8, and 1, 3, and 5 mg/L of CCM-Co-ZIF-8 on the growth of RAW264.7 and L929 cells were tested using the CCK-8 cell viability assay kit. The cells were incubated with the materials for a duration of 72 h in a coculture setup, and the CCK-8 assay was performed every 24 h. Following a 2 h incubation with the CCK-8 substance, the optical density at 450 nm was measured using a plate reader to determine cell viability. At the end of a 72 h period, cell viability was further assessed utilizing the Calcein AM/PI cell health and toxicity detection kit. The cells were exposed to Calcein AM/PI buffer for 30 min, and subsequently, the staining results of live and dead cells were observed under a fluorescence microscope.

2.9. Adsorption Energy Calculation Method. The magnitude of the adsorption energy determines whether a reaction can occur spontaneously. In cases where the adsorption energy exceeds 0, the reaction is impeded. If the adsorption energy is below 0, then the reaction could occur spontaneously. The formula for calculating adsorption energy is as follows

$$\Delta E_{ads} = \frac{E_{slab}}{\text{adsorbate}} - E_{slab} - E_{adsorbate}$$

where ΔE_{ads} is the adsorption energy in kcal/mol; the total energy of the system, including the crystal surface and activated adsorbate, is referred to as the E_{slab}/adsorbate, in kcal/mol; E_{slab} is the total energy of the crystal surface before the reaction, in kcal/mol; and $E_{adsorbate}$ is the energy of adsorbate on the surface before the reaction, in kcal/mol.

2.10. Cellular Antioxidative Capacity. Raw264.7 cells were seeded in a 6-well plate with 2 mL of culture medium at a density of 1 $\times 10^6$ cells/mL per well and incubated for 24 h. LPS (200 ng/mL) and interferon-γ (30 ng/mL) were added to the RAW264.7 cells, followed by 24 h of incubation. Subsequently, CCM (6 μmol/L), Co-ZIF-8 (10 mg/L), and CCM-Co-ZIF-8 (4.5 mg/L) were added to the cells and cocultured for 24 h before conducting PCR amplification. The relative expression of the synthesized mRNA (iNOS and Mrc1, with β-actin as reference) was compared to that of the control group.

2.11. Mice Experiments. The animal experiments were performed at Yangzhou University in accordance with the "Guidelines for Care and Use of Experimental Animals at Yangzhou University" and were approved by the Animal Welfare and Ethics Committee of the university (DWLL-202202-029). The supervision and inspection of animal experiments are under the responsibility of the Animal Welfare and Ethics Committee of Yangzhou University. For this study, we used 8 week old Balb/c mice with an average weight of 20 g. The mice were maintained at a temperature of 22 °C, a relative humidity of approximately 55%, and a 12 h light−dark cycle. The mice were categorized into four groups: normal

https://doi.org/10.1021/acsomega.4c02446
ACS Omega 2024, 9, 30571−30582

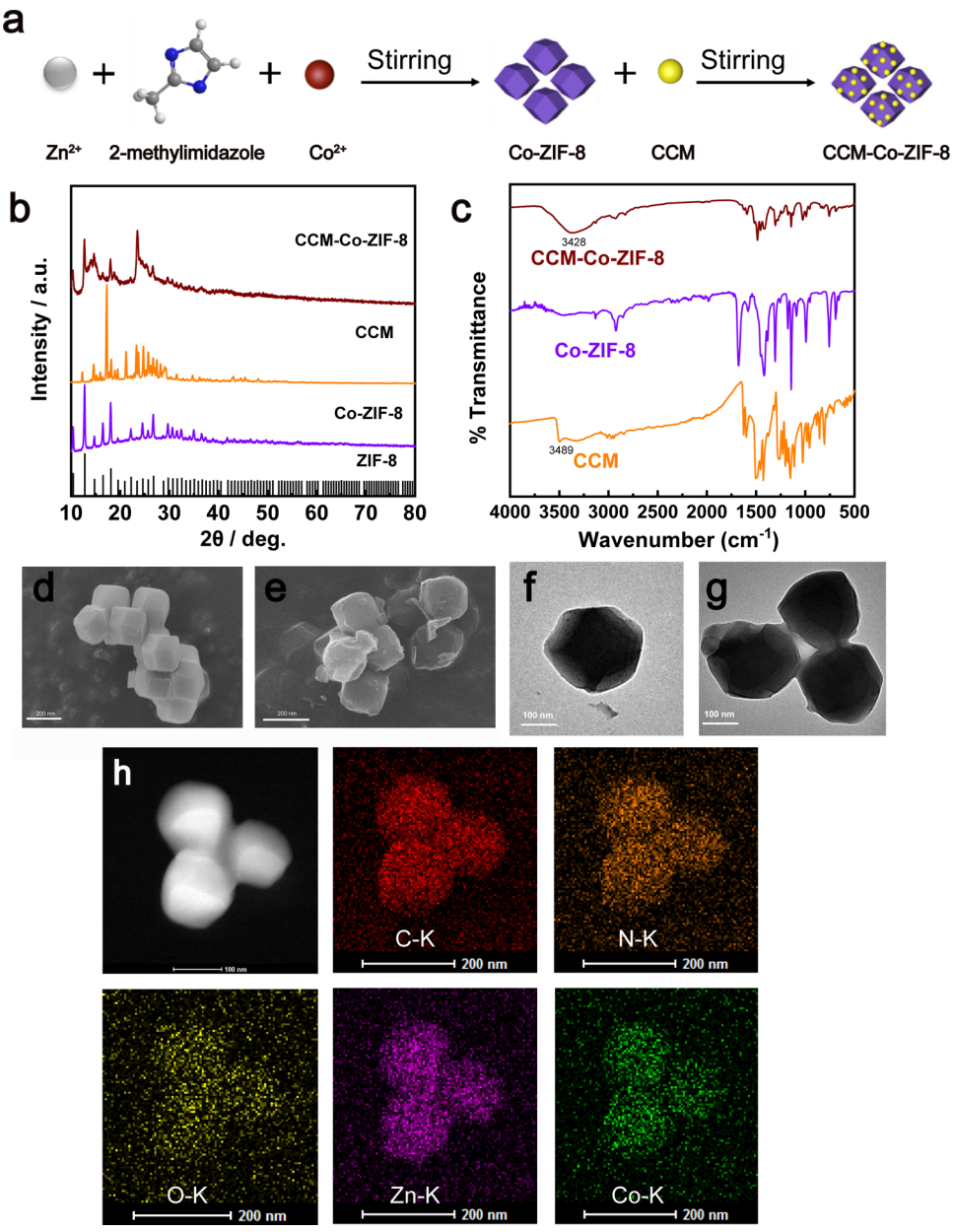

Figure 2. (a) Diagram for the CCM-Co-ZIF-8 synthesis. (b) X-ray diffraction (XRD) pattern of the samples. (c) Fourier transform infrared (FTIR) spectrum of the samples. (d, e) SEM images of Co-ZIF-8 and CCM-Co-ZIF-8. (f, g) The TEM images of Co-ZIF-8 and CCM-Co-ZIF-8. (i) EDX element mapping image of CCM-Co-ZIF-8.

control group, CCM-Co-ZIF-8 pure drug group, DSS-induced colitis group, and DSS-induced CCM-Co-ZIF-8 treatment group. Each group consisted of 10 mice. In the DSS-induced colitis group and DSS-induced CCM-Co-ZIF-8 treatment group, the drinking water was replaced with DSS dispersion in ddH_2O to induce colitis in the mice for 7 days. The normal control group and CCM-Co-ZIF-8 pure drug group received normal sterile drinking water. Starting from day 8, the CCM-Co-ZIF-8 pure drug group and DSS-induced CCM-Co-ZIF-8 treatment group were orally administered CCM-Co-ZIF-8 (10 mg/kg) daily, while the other two groups were administered an equivalent volume of saline solution by oral gavage. On day 15, all mice were humanely euthanized while under anesthesia induced by isoflurane, and their entire colons were extracted. The colonic length was measured, and then, it was carefully rinsed with physiological saline. A section of the colon was prepared for histological examination. The heart, liver, spleen, lung, and kidney were obtained for subsequent pathological analysis. During the 8 day period, visible fecal consistency, weight changes, and fecal bleeding were assessed daily. Disease activity index (DAI) was measured, which included fecal consistency index (0−3), weight loss index (0−4), and fecal bleeding index (0−3).

2.12. PCR. Total RNA was extracted from colonic tissues of experimental animals (100 mg) using the Trizol reagent (Takara). The tissue was cut into small pieces using scissors and then homogenized by repeatedly injecting it with a 10 mL syringe. Subsequently, 600 μL of Trizol reagent was added, and the mixture was vigorously shaken for 15 s followed by a 5 min incubation. Finally, 120 μL of chloroform was added, and the solution was shaken again before being allowed to stand, vigorously shaking, followed by centrifugation (12 000 rpm, 4

https://doi.org/10.1021/acsomega.4c02446
ACS Omega 2024, 9, 30571−30582

°C, 10 min) to collect the RNA-containing supernatant. An equal volume of isopropyl alcohol was added, followed by shaking and centrifugation (12 000 rpm, 4 °C, 10 min). The RNA pellet was washed with 500 μL of 75% ethanol prepared with DEPC water, followed by centrifugation (7500 rpm, 4 °C, 5 min), discarding the ethanol, air-drying the pellet, and resuspended in 20 μL of DEPC water for measurement of RNA concentration and purity. cDNA synthesis was performed using the PrimeScript II first Strand cDNA Synthesis Kit (Takara), and the primers were synthesized by a Sangon Biotech as shown in Table S1. β-Actin was used as the reference gene. The conditions of PCR were as follows: maintenance time, 2 min at 95 °C, PCR stage 95 °C for 15 s, 60 °C for 15 s, 72 °C for 30 s, a total of 45 cycles. Melting curve stage, 95 °C 15 s, 60 °C 15 s, 95 °C 15 s. Synthetic mRNA was expressed normalized to controls by β-actin mRNA. The expression levels of iNOS, MrC1, and β-actin were detected, and the expression levels of target genes were calculated by $2^{-\Delta\Delta Ct}$.

2.13. Immunofluorescence. The tissue specimens from the normal control group, DSS-induced colitis group, and DSS-induced CCM-Co-ZIF-8 treatment group were fixed in a 10% formalin solution. The thickness of the sections was 6 μm. The sections were incubated in 0.25% Triton PBS solution at room temperature for 25 min, followed by three washes with PBS (5 min each). Subsequently, the tissue sections were blocked with 10% bovine serum albumin (BSA) solution in PBS for 30 min at room temperature and then washed three times with PBS for 5 min each wash. The diluted primary antibodies against CD68 (rabbit, 1:2000) and CD163 (rabbit, 1:2000) in 10% goat serum were applied to the sections, with 10% goat serum serving as a negative control. After three washes with PBS for 5 min each, the sections were incubated with Alexa 488-conjugated secondary antibodies and Alexa 568-conjugated secondary antibodies diluted in PBS at a ratio of 1:500, along with a mixture of secondary antibodies as a negative control. After incubation at 37 °C for 2 h, the sections were washed three times with PBS for 10 min each, followed by DAPI counterstaining of cell nuclei for 30 min. Then, the sections were washed three times with PBS for 5 min each. Finally, the sections were mounted with a fluorescence mounting medium and observed under an inverted fluorescence microscope.

2.14. In Vivo Biosafety Testing. Colons from the normal control group, CCM-Co-ZIF-8 pure drug group, DSS-induced colitis group, and DSS-induced CCM-Co-ZIF-8 treatment group underwent fixation in 10% formalin and embedding in OCT embedding medium. Subsequently, hematoxylin and eosin (H&E) staining was performed, and the morphological changes were observed under an optical microscope. For the Balb/C mice subjected to weight measurement and histopathological examination, blood samples were collected from the orbital cavity. Hematological and serum biochemical parameters of the mice in the normal control group, CCM-Co-ZIF-8 pure drug group, and DSS-induced CCM-Co-ZIF-8 treatment group were determined. The hematological parameters encompassed measurements of erythrocytes, leukocytes, hemoglobin levels, and platelet counts. The evaluations of alanine transaminase (ALT), aspartate transaminase (AST), and blood urea nitrogen (BUN) levels were included in the serum biochemical parameters. The existing literature was consulted to conduct a comprehensive analysis of the recorded parameters. Additionally, samples of heart, liver, spleen, lung, and kidney tissues were obtained, washed with deionized water, and fixed in a 10% neutral buffered formalin. After routine processing, the samples were embedded in an OCT embedding medium. Subsequently, the tissues were sectioned to a thickness of 6 μm, stained with H&E, and the morphological changes were observed under an optical microscope. This was carried out to evaluate the potential in vivo toxicity of CCM-Co-ZIF-8 on major organs.

3. RESULTS AND DISCUSSION

3.1. Synthesis and Structure Characterization of Co-ZIF-8 and CCM-Co-ZIF-8. As shown in Figure 2a, 1.161 g of 2-methylimidazole was dissolved in 10 mL of DMF−methanol mixture. Simultaneously, 0.535 g of $Zn(NO_3)_2{\cdot}6H_2O$ and 0.535 g of $Co(NO_3)_2{\cdot}6H_2O$ were dissolved in 15 mL of DMF−methanol mixture. The solution of 10 mL of 2-methylimidazole was then dropped into 15 mL of $Zn(NO_3)_2{\cdot}6H_2O$ and $Co(NO_3)_2{\cdot}6H_2O$ solution to obtain Co-ZIF-8. After dispersing Co-ZIF-8 uniformly, CCM was added to obtain CCM-Co-ZIF-8. Figure 2b shows the XRD spectra of CCM, Co-ZIF-8, and CCM-Co-ZIF-8. The peaks at 2θ values of 7.29, 10.44, 12.83, and 18.10° could be assigned to the (110), (200), (211), and (222) crystal planes of Co-ZIF-8, respectively. These peak positions align precisely with the standard card of ZIF-8, providing strong evidence of the successful synthesis of Co-ZIF-8. The peak at approximately 2θ of 15.5° in the CCM-Co-ZIF-8 spectrum is attributed to CCM, confirming the effective binding of CCM with the Co-ZIF-8 matrix. In the FTIR spectrum of CCM-Co-ZIF-8 (Figure 2c), the peaks at 3426 and 3055 cm^{-1} correspond to the stretching vibrations of aromatic C−H and aliphatic C−H bonds, respectively. Meanwhile, vibrations of aliphatic C−C, C−N, C−O, and C−O−C bonds are observed at 2359, 1605, 1184, and 894 cm^{-1}, respectively. This provides valuable insights into the spectral characterization of the compounds under investigation. The relocation of the curcumin phenolic group stretching peak from 3489 to 3428 cm^{-1} observed in CCM-Co-ZIF-8 might suggest the encapsulation of curcumin within the Co-ZIF-8 framework.[27,28] As shown in Figure S1, the characteristic Raman signals of Co-ZIF-8 (≈685, 1147, 1180, and 1456 cm^{-1}) disappear on CCM-CO-ZIF-8, indicating that CCM is successfully coated on Co-ZIF-8.

The average size of the surface-synthesized Co-ZIF-8 particles determined by the nanometer estimation of SEM measurements is approximately 150 nm, with some particles reaching sizes of 170 nm with the primary morphology of rhombic dodecahedron (Figure 2d,e). After loading curcumin, irregularities together with a slight increase in particle size are observed at the periphery of the material compared to uncoated Co-ZIF-8. In agreement with SEM results, TEM photos indicate that Co-ZIF-8 is a rhombic dodecahedral particle with a size of approximately 150 nm (Figure 2f,g). The results obtained from particle size measurements are approximately 160 nm, which is consistent with the SEM and TEM results (Figure S2). The surface of the Co-ZIF-8 material is smooth with a well-defined crystallinity. After loading CCM, the morphology of the material becomes slightly rounder and the size has slightly increased, approximately 1.3 times larger than before. The distribution of C, N, O, Co, and Zn on the surface of CCM-Co-ZIF-8 can be observed from the EDX mapping diagram (Figure 2i). As shown in Table S2, the ζ-potential results of Co-ZIF-8 and CCM-Co-ZIF-8 indicate that the coating of CCM has little influence on the particle

https://doi.org/10.1021/acsomega.4c02446
ACS Omega 2024, 9, 30571−30582

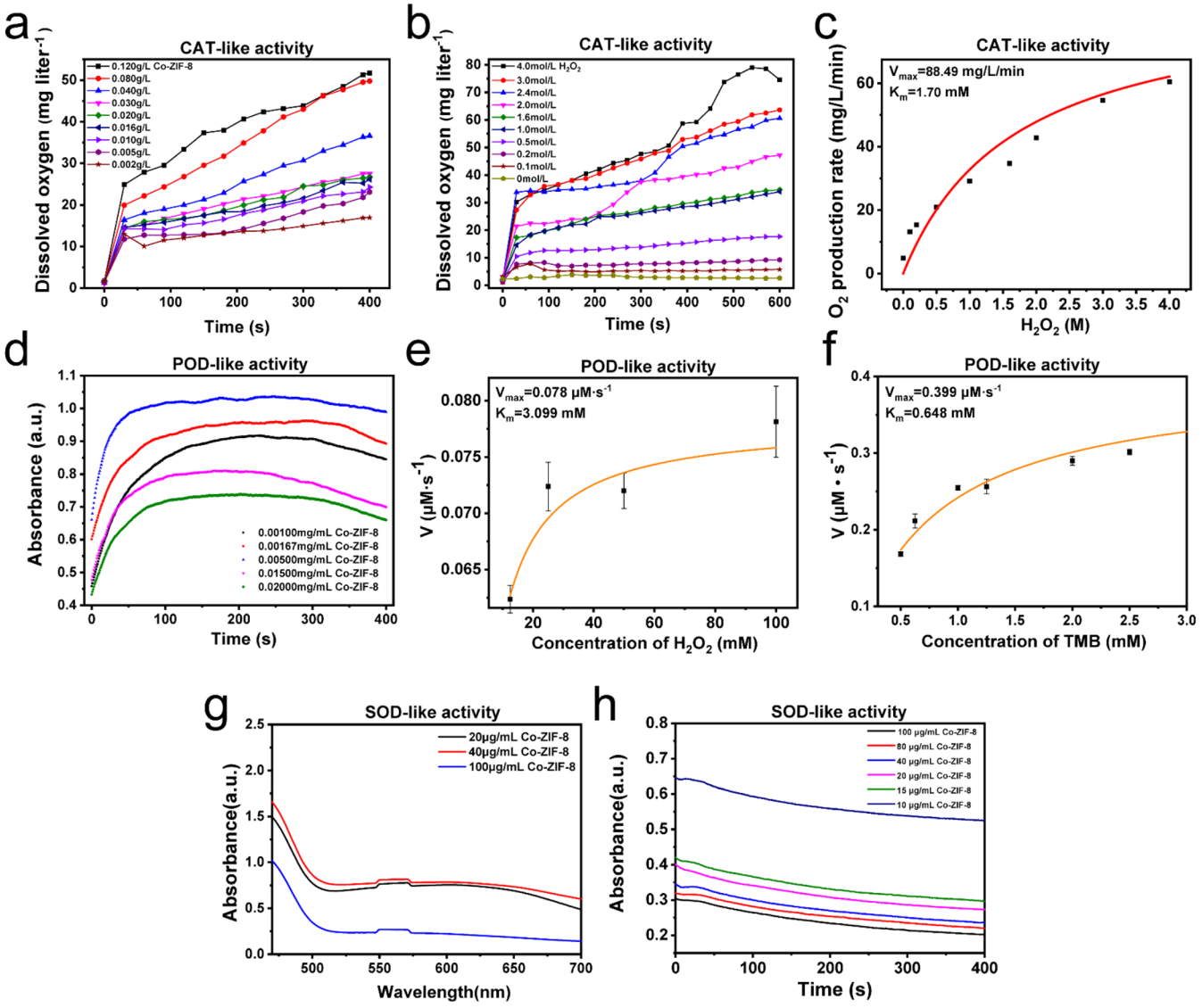

Figure 3. (a) Effect of different concentrations of Co-ZIF-8 on H_2O_2 removal; (b) the effect of different concentrations of hydrogen peroxide on H_2O_2 removal; (c) steady-state kinetics measurement of catalase-like activity of Co-ZIF-8 at different H_2O_2 concentrations; (d) the effect of different concentrations of Co-ZIF-8 on H_2O_2 removal; (e) steady-state kinetics measurement of peroxidase-like activity of Co-ZIF-8 at different H_2O_2 concentrations (0.3−60 mM); (f) steady-state kinetic determination of peroxidase-like activity of Co-ZIF-8 at different TMB concentrations (6−120 mM); (g) the effect of different concentrations of Co-ZIF-8 on $^{\bullet}O_2^-$ removal; and (h) time-dependent absorbance at 550 nm of NBT in the presence of different concentrations of Co-ZIF-8.

charge results, with similar potential results observed in both inflammatory and neutral environments.

3.2. In Vivo ROS Scavenging Capability of Co-ZIF-8. *3.2.1. CAT-like Enzyme-like Activity of Co-ZIF-8.* H_2O_2 is a powerful oxidizing agent and a downstream product of $^{\bullet}O_2^-$. In biological systems, enzyme catalase (CAT) facilitates the decomposition of H_2O_2 into H_2O and O_2. This study aimed to evaluate the activity of nanozymes with CAT-like properties of Co-ZIF-8 by measuring the production of oxygen during H_2O_2 decomposition. As shown in Figure 3a, a positive correlation between the concentration of Co-ZIF-8 and its CAT-like activity is observed on the basis of the initial rate of oxygen evolution within 400 s. Figure 3b presents the rate of O_2 generation at different concentrations of H_2O_2 in the presence and absence of Co-ZIF-8. Notably, gas bubbles were observed in the reaction solution, and an increased Co-ZIF-8 concentration led to a gradual increase in the dissolved oxygen levels. The CAT enzyme activity of Co-ZIF-8 followed the Michaelis−Menten kinetics (Figure 3c), allowing the determination of crucial enzymatic parameters such as the Michaelis−Menten constant (K_m = 1.7 mM) and maximum initial velocity (V_{max} = 88.49 mg/L). These values underscore the robust CAT-like activity of Co-ZIF-8. To explore oxygen generation in a weakly acidic environment resembling an inflammatory microenvironment, additional investigations were conducted. It is evident that a higher amount of O_2 was produced under acidic conditions compared to typical physiological conditions (Figure S3). Specifically, between 50 and 400 s of the reaction, the amount of oxygen generated under acidic conditions was approximately 1.8 times higher than that generated under neutral conditions. This observation provides additional confirmation of the material's pH-responsive characteristics.

3.2.2. POD-like Enzyme-like Activity of Co-ZIF-8. Peroxidase (POD) enzyme could catalyze H_2O_2 or $^{\bullet}OH$ into H_2O.

https://doi.org/10.1021/acsomega.4c02446
ACS Omega 2024, 9, 30571−30582

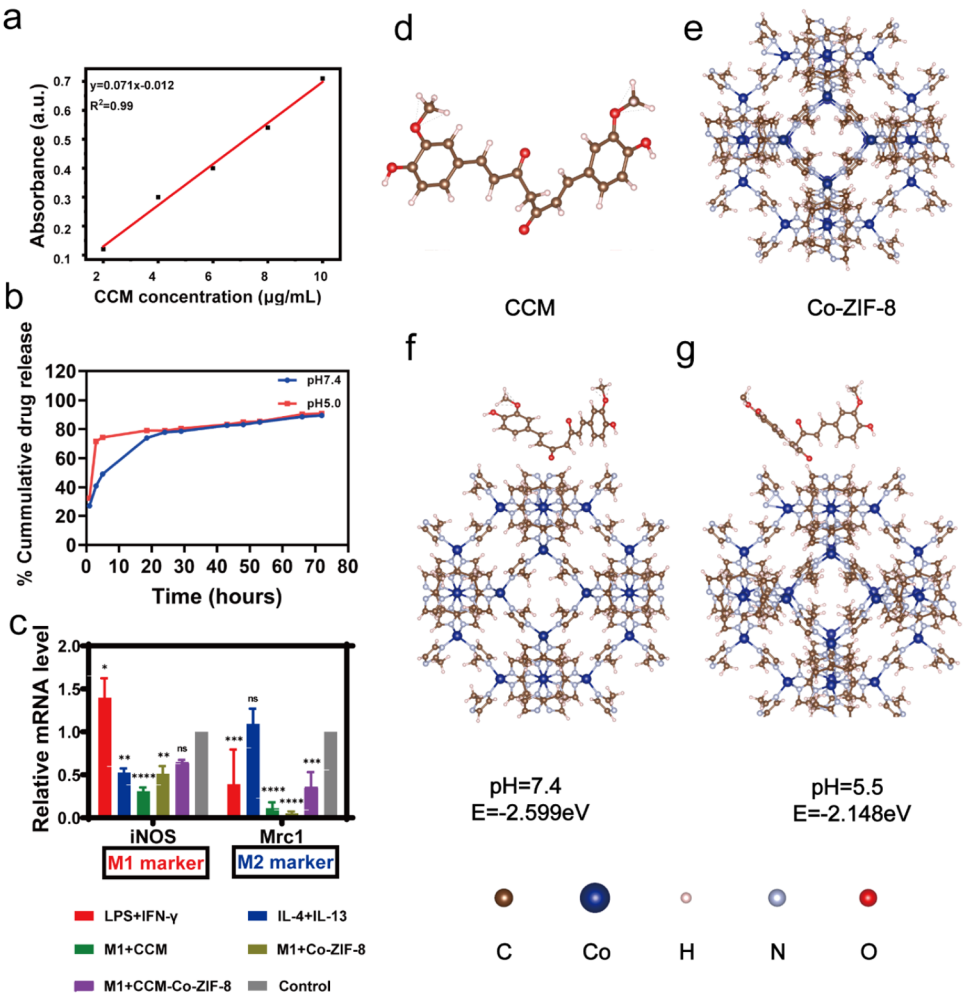

Figure 4. (a) Drug release profiles of CCM. (b) Drug release curves of CCM-Co-ZIF-8 at different pH values. (c) mRNA expression levels of M1 macrophage marker (iNOS) and M2 macrophage marker (Mrc1) in RAW264.7 cells under different conditions (n = 3). (d) Structure chart of CCM. (e) Structure chart of Co-ZIF-8. (f) The structure of CCM-Co-ZIF-8 with pH equal to 7.4. (g) The structure of CCM-Co-ZIF-8 with pH equal to 5.5. For all of the analyses, multiple comparison one-way analysis of variance followed by Dunnett's test was conducted. The following statistical symbols were used to indicate the level of significance: *p < 0.05, **p < 0.01, ***p < 0.001, ****p < 0.0001. The abbreviation "ns" was used to indicate nonsignificance.

Such enzyme activity of Co-ZIF-8 was characterized via a colorimetric assay by recording the nanomaterial concentration-dependent absorbance values (652 nm) of standard sensor TMB in weak acidic conditions.[29] The results indeed indicate the POD activity of Co-ZIF-8 (Figure S4). Furthermore, the results demonstrated that an increase in the POD activity of Co-ZIF-8 is in positive correlation with the concentration (Figure 3d). The corresponding Michaelis–Menten curves are shown in Figure 3e,f, utilizing H_2O_2 and TMB as substrates, respectively. The K_m values for Co-ZIF-8 were determined to be 2.262 and 2.092 mM, while the corresponding V_{max} values were 1.517 and 0.887 μM s^{-1}, respectively. These experimental findings strongly support the outstanding ROS scavenging capability of Co-ZIF-8, showcasing its potential for anti-inflammation treatment.

3.2.3. SOD-like Enzyme-like Activity of Co-ZIF-8. NBT is a sensitive indicator for superoxide anion ($^{\bullet}O_2^-$) and could show absorption at 550 nm upon reaction with $^{\bullet}O_2^-$[30]. Figure 3g demonstrates that Co-ZIF-8 has significant $^{\bullet}O_2^-$ scavenging activity. The removal rate of $^{\bullet}O_2^-$ progressively increases with an increasing Co-ZIF-8 concentration within a specific range. The highest $^{\bullet}O_2^-$ removal ability is observed at a Co-ZIF-8 concentration of 100 μg/mL. Through the measurement of the absorbance variation at 550 nm (Figure 3h), the superoxide dismutase SOD-like activity positively correlates with the Co-ZIF-8 concentration. Hence, Co-ZIF-8 exhibits a favorable SOD-like activity by catalyzing the generation of H_2O_2 and O_2 from $^{\bullet}O_2^-$.

3.3. Drug Loading and Release Properties of Co-ZIF-8. Figure 4a illustrates the standard linear curve for curcumin release, with formulas of $Y = 0.071X - 0.012$ obtained through the dialysis-based measurement of various curcumin concentrations using a UV spectrophotometer. To achieve complete dissolution of loaded curcumin, CCM-Co-ZIF-8 was treated with a little amount of hydrochloric acid, resulting in a characteristic absorbance value of 2.12. Utilizing the standard curve, the drug loading capacity was determined as 30.03 mg/mL, corresponding to an encapsulation efficiency of 60.06%. Due to the mildly acidic properties of inflamed tissues, the study primarily centered on the pH-responsive drug delivery characteristics of CCM-Co-ZIF-8, specifically under in vitro conditions with acidic pH levels (pH 5.0 and pH 7.4). Over time, absorbance at 425 nm gradually increased. Within 20 h, CCM demonstrated an enhanced release under acidic

https://doi.org/10.1021/acsomega.4c02446
ACS Omega 2024, 9, 30571−30582

conditions, while little discrepancy in the cumulative release after 72 h was observed between the two environments (Figure 4b). This phenomenon can be attributed to the instability of Co-ZIF-8 in the PBS aqueous solution, where strong inorganic substances competitively attack the coordination bonds between zinc and 2-methylimidazole, leading to the degradation of Co-ZIF-8. Consequently, rapid drug release occurs, indicating that Co-ZIF-8 would not effectively enhance the sustained-release effect of CCM treatment.

3.4. Cytotoxicity Assay. We employed the CCK-8 method to assess the cell toxicity of CCM, Co-ZIF-8, and CCM-Co-ZIF-8 using the L929 and RAW264.7 cell lines as model systems. The cells were cultured for a duration of 72 h, with CCK-8 assay conducted every 24 h to evaluate cell viability (Figure S5). Pure curcumin showed no significant cellular toxicity at concentrations below 8 μmol/L even when the incubation period was extended to 72 h. The cell viability remained near 100% during this period. Co-ZIF-8 exhibited a slight decrease in cell viability in L929 cells with noticeable cytotoxicity observed at a concentration of 5 mg/L. However, it did not exert significant cytotoxic effects on RAW264.7 cells. CCM-Co-ZIF-8 displayed no significant cytotoxicity with concentrations below 5 mg/L. In the presence of L929 cells, materials displayed acceptable cell cytotoxicity after 72 h of incubation. These findings indicate that CCM, Co-ZIF-8, and CCM-Co-ZIF-8 are feathered with favorable biocompatibility, meeting the requisite criteria for further applications in biomedical materials.

3.5. Gene Phenotype Analysis of the Anti-Inflammatory Effect of CCM-Co-ZIF-8 on RAW264.7 Cells. Macrophages are the primary inflammatory and immune cells, and the pathogenesis of colitis is associated with the infiltration of inflammatory cells, particularly M1 macrophages.[31] These macrophages are formed in response to various biological cues, including excessive ROS. Figure 4c demonstrates the in vitro anti-inflammatory effects of CCM-Co-ZIF-8 on RAW264.7 mouse monocytic macrophages, which is crucial for evaluating the anti-inflammatory activity of CCM-Co-ZIF-8 on activated macrophages. To examine the impact of CCM-Co-ZIF-8 on macrophage phenotypes, we first induced M0 macrophages to become M1 macrophages using LPS and IFN-γ. After 24 h of coincubation with M1 macrophages, the cells were treated with pure curcumin, Co-ZIF-8, and CCM-Co-ZIF-8. Quantitative PCR analysis demonstrated a notable increase in the expression of the proinflammatory cytokine Inducible nitric oxide synthase (iNOS) was exposed to LPS and IFN-γ. However, M1 macrophages treated with CCM-Co-ZIF-8 exhibited a significant decrease in iNOS expression levels compared to the control group, albeit less effective than Co-ZIF-8 alone. Interestingly, curcumin itself was found to downregulate M1-associated genes, and its effect was superior to that of CCM-Co-ZIF-8. This suggests that the decoration of curcumin with Co-ZIF-8 might inhibit the functionality of CCM. However, there was no significant anti-inflammatory effect, indicating that CCM-Co-ZIF-8 can only suppress the expression of proinflammatory cytokines.

3.6. Density Functional Theory Calculation. To explore the interaction between the CCM and Co-ZIF-8, density functional theory calculations were performed. The essential calculations for this research were performed with the Vienna Ab initio Simulation Package (VASP). VASPsol was utilized to simulate the behavior of these materials in solution, enabling the consideration of solvent molecules' influence on their electronic structure and energy characteristics. The electronic exchange−correlation energy calculation utilized the generalized gradient approximation (GGA) method. The study carefully considered potential adsorption sites and the posture configurations of adsorbed molecules, ensuring that all structures maintained symmetry while undergoing adequate relaxation. The binding sites were predicted based on the lowest energy, as demonstrated in the provided diagram. Given the acidic nature often present in inflammatory environments, binding energies were meticulously calculated under both physiological (pH = 7.4) and acidic conditions (pH = 5.5) to evaluate the interaction strength between CCM and Co-ZIF-8. Results indicated that at physiological pH, the observed binding energy was −2.599 eV, whereas under the acidic conditions mimicking an inflammatory environment, it decreased to −2.148 eV. This notable difference strongly suggests that the lower pH in inflammatory conditions impacts the protonation state of CCM molecules, altering their charge distribution and electron cloud density. In such acidic conditions, certain initially neutral functional groups may become protonated, acquiring a positive charge. This protonation shift could weaken the electrostatic interactions between CCM molecules and Co-ZIF-8, leading to a reduced overall binding energy. Consequently, the interaction between CCM and Co-ZIF-8 is diminished, resulting in a lower binding energy. This discovery offers significant molecular-level insights into the interactions of CCM with Co-ZIF-8 under different pH conditions and provides a theoretical foundation for the potential use of CCM as a therapeutic agent in inflammatory environments.

3.7. In Vivo Toxicity. After 1 week of monitoring body weight, Balb/C mice were orally administered with 10 mg/kg of CCM-Co-ZIF-8 on a daily basis, and their hematological parameters were evaluated. The findings indicated that the administration of oral CCM-Co-ZIF-8 did not result in any notable variances in the white blood cell count, red blood cell count, or platelet count among the treated mice (Figure S6). These parameters remained within the normal range, indicating the absence of systemic infections, anemia, or abnormalities in the hemostasis function as a result of the CCM-Co-ZIF-8 administration. It can be inferred that the oral administration of CCM-Co-ZIF-8 does not cause any notable alterations in routine blood tests. Furthermore, H&E staining and tissue weight analysis were conducted on various organs including the heart, liver, spleen, lungs, and kidneys of the mice. The observations demonstrated that CCM-Co-ZIF-8 did not induce any apparent damage to these organs. Morphologically, H&E staining of organs from mice receiving oral CCM-Co-ZIF-8 showed no evidence of inflammatory cells or tissue damage (Figure S7). These pathological findings confirm the excellent biocompatibility and low systemic toxicity of synthesized CCM-Co-ZIF-8, underscoring its potential for biomedical applications.

3.8. In Vivo Anti-Inflammatory Performance. The DSS-induced model is widely used in inducing UC due to its simplicity and high success rate.[32] Characteristics of DSS-induced mouse UC include significant weight loss, diarrhea, and severe bloody stools. In this experiment, random assignment was used to allocate animals into four groups; the groups consisted of the CCM-Co-ZIF-8 group, DSS group, and DSS + CCM-Co-ZIF-8 group. The administration of ddH_2O DSS dispersion starts from −7 day. Diminished

https://doi.org/10.1021/acsomega.4c02446
ACS Omega 2024, 9, 30571−30582

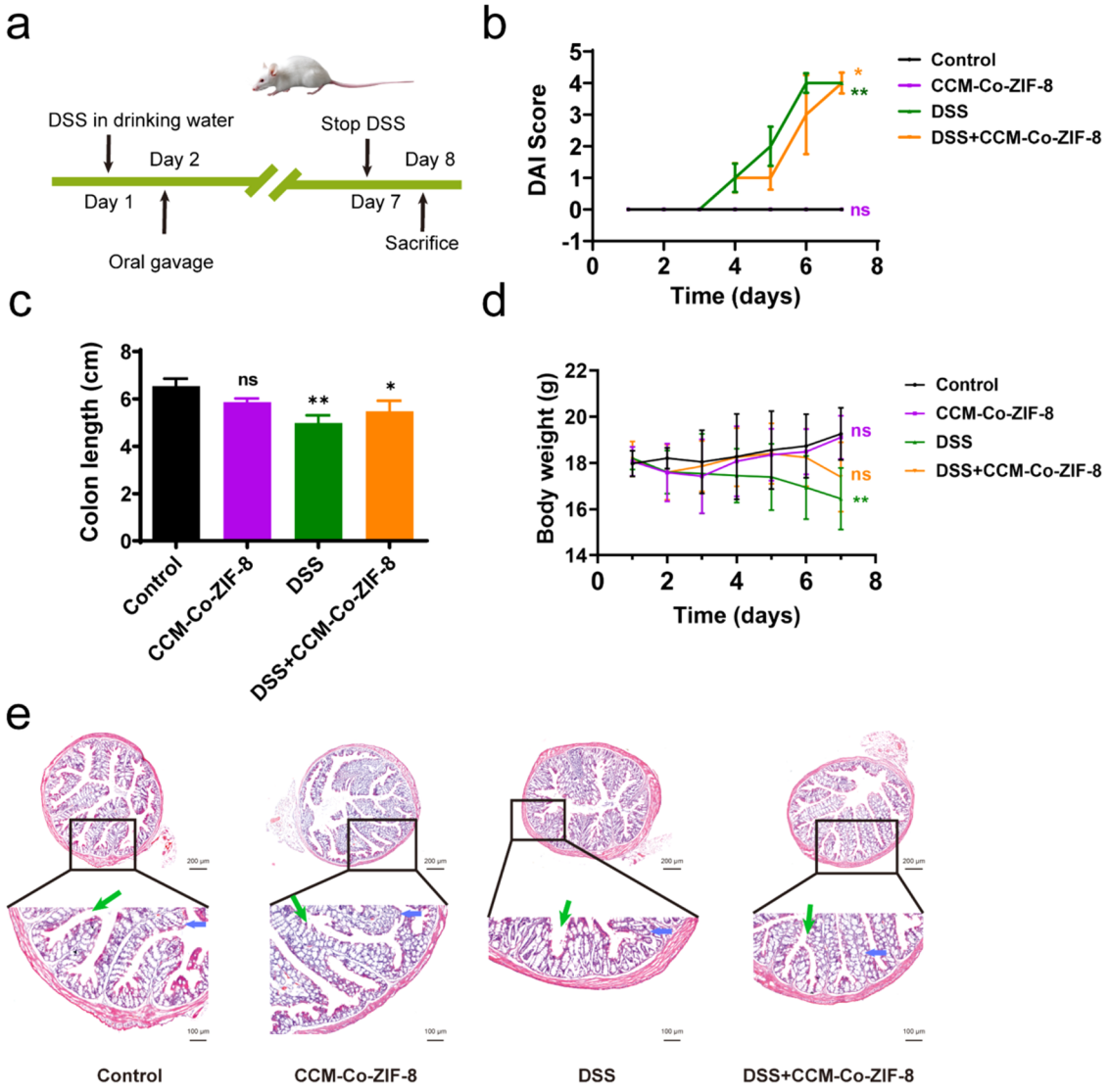

Figure 5. (a) Diagram illustrating the design of animal experiments. (b) The score for the disease activity index (DAI). (c) Colon length. (d) Body weight change. (e) Colonic tissue H&E staining: the green arrow points to the recess branch, and the purple arrow points to the goblet cell. In all analyses, a one-way analysis of variance was conducted, followed by Dunnett's test for multiple comparisons. Statistical significance levels were indicated by $*p < 0.05$, $**p < 0.01$ ($n = 3$), while nonsignificant results were denoted by the abbreviation "ns".

appetite and loose stool appeared on day −4 of the modeling process, followed by a noticeable weight loss on −2 day. Different levels of diarrhea and significant rectal bleeding were detected, confirming the successful creation of a mouse model of ulcerative colitis induced by DSS. The mice in the initial two groups were given normal saline. In the DSS + CCM-Co-ZIF-8 group, from the second day onward, a daily oral dose of 10 mg/kg of CCM-Co-ZIF-8 was administered to one group, while the remaining groups received the same volume of normal saline to maintain consistent external stimulation in all mice (Figure 5a). Several metrics were monitored to evaluate the efficacy of the therapy, encompassing parameters such as animal mass, size of the colon, incidence of hemorrhages, DAI, histopathological features indicating inflammation, and the extent of expression of cytokines affiliated with inflammatory reactions.

3.8.1. Physiological Parameters of Colitis Mice. DAI serves as a crucial metric in the assessment of the intensity of colitis induced by DSS in mice.[33] DAI scoring system outlined in Table S3 was employed to evaluate the severity of the lesions in the colitis model. Figure 5b demonstrates the impact of CCM-Co-ZIF-8 on colitis modeling in mice. In the control group, mice exhibited normal physiological conditions with consistent weight gain, normal stool color and shape, and no diarrhea or blood stools. The DSS group showed signs of loose and bloody stool starting from the third day of modeling along with a significant increase in the DAI index, indicating successful colitis modeling. The DSS + CCM-Co-ZIF-8 group exhibited symptoms similar to those of the DSS group during the modeling period. However, in the later stages of treatment, CCM-Co-ZIF-8 demonstrated therapeutic effects, leading to a notable improvement in disease symptoms and a significant reduction in the DAI index. These results suggest that CCM-Co-ZIF-8 has a certain therapeutic efficacy in treating colitis in mice. As shown in Figure 5c, compared with the control group, DSS-induced mice exhibited a significant reduction in colon length (4.98 ± 0.33 cm vs 6.54 ± 0.31 cm, $p < 0.001$). However, in the DSS + CCM-Co-ZIF-8 group, the phenomenon of colon shortening became less pronounced.

https://doi.org/10.1021/acsomega.4c02446
ACS Omega 2024, 9, 30571−30582

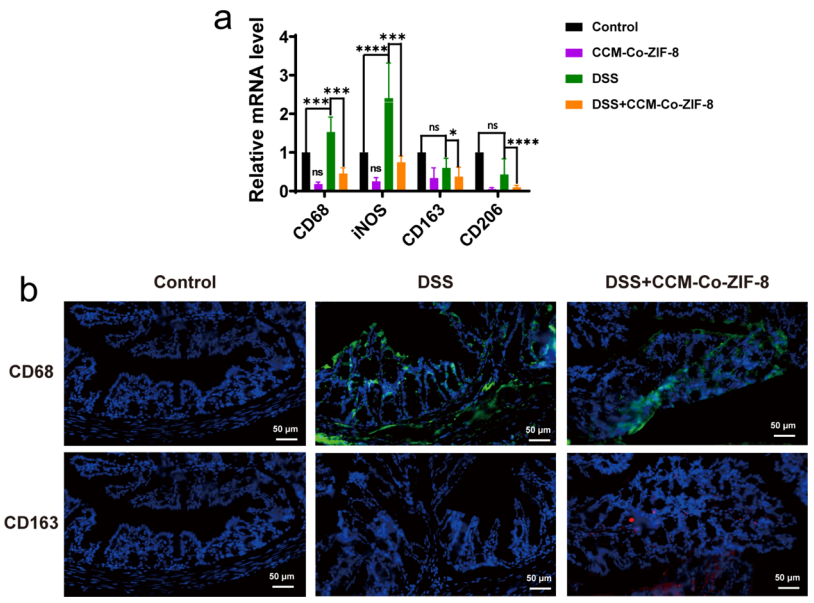

Figure 6. (a) Effect of CCM-Co-ZIF-8 on the expression of inflammatory genes in the colonic tissue of mice with colitis ($n = 3$). (b) The effect of CCM-Co-ZIF-8 on the localization expression of inflammatory proteins in the colonic tissue of mice with colitis. A multiple comparison one-way analysis of variance was conducted for all analyses, followed by Dunnett's test. The level of significance was denoted by the symbols *$p < 0.05$, ***$p < 0.001$, and ****$p < 0.0001$, while the abbreviation "ns" indicated nonsignificance.

Compared to the DSS group, the colon length in the CCM-Co-ZIF-8 group increased by 9.94% ($p < 0.05$, Figure S8).

The systemic malnutrition caused by UC leads to a rapid weight loss. It can be seen that in the experiment evaluating the effect of CCM-Co-ZIF-8 on mice with colitis, the mice in the control group showed a slow weight gain in the first 3 days and a significant upward trend starting from the fourth day. By the end of the experiment, the weight of the mice in the control group increased by 7.16%, indicating their healthy growth. As shown in Figure 5d, the DSS group exhibited a slow upward trend in weight for the first 3 days, followed by a continuous decline from the fourth day. The DSS+CCM-Co-ZIF-8 group showed a slow upward trend in weight for the first 4 days and then gradually decreased but at a slower rate compared to the DSS group. Statistical analysis revealed a remarkably significant distinction ($p < 0.01$) between the DSS group and the control group. Throughout the duration of the experiment, the mice in the DSS + CCM-Co-ZIF-8 group consistently exhibited significantly higher body weights compared to those in the DSS group, indicating the effective mitigation of weight loss induced by colitis in mice by CCM-Co-ZIF-8.

3.8.2. Inflammatory Tissue Histological Changes. To further investigate the therapeutic efficacy of CCM-Co-ZIF-8 in mouse colitis, we collected colon tissues and performed H&E staining to observe the histopathological changes. The results revealed that the colon tissues of the control group mice appeared intact, with intact mucosal structures; the deep narrowing of the intestinal crypts indicated by the green arrow in Figure 5e remains intact, while the abundant goblet cells indicated by the purple arrow, and no signs of edema or inflammatory cell infiltration. The colon tissues of the DSS group mice exhibited severe damage, characterized by the disrupted mucosal cell arrangement, necrosis, and epithelial loss; after damage, there is a reduction in the branching of the crypts indicated by the green arrow, a significant decrease in goblet cells indicated by the purple arrow, and a prominent infiltration of inflammatory cells. Comparatively, the colon sections of the DSS+CCM-Co-ZIF-8 group mice showed improved structural integrity compared with the DSS group. Only mild inflammation was observed, with the colon tissue's mucosal structure remaining intact and a significant reduction in inflammatory cell infiltration. These findings imply that CCM-Co-ZIF-8 demonstrates promise as a potential therapeutic intervention for the management of colitis in mice.

3.8.3. Therapeutic Effects of Inflammation at the Genetic Level. CD68 and iNOS are proinflammatory cytokines, while CD163 and CD206 are anti-inflammatory cytokines that play important roles in controlling inflammation and immune response.[34,35] In order to explore the potential protective effect of CCM-Co-ZIF-8 against DSS-induced colitis in mice, the expression levels of CD68, iNOS, CD163, and CD206 were assessed. As shown in Figure 6a, in the CCM-Co-ZIF-8 treatment experiment, the expression levels of the CD68 and iNOS genes in the DSS group were increased by 0.52- and 1.4-folds, respectively, compared to the control group. In contrast, after treatment with CCM-Co-ZIF-8, the expression levels of the CD68 and iNOS genes decreased by 70 and 57.1%, respectively, compared to the DSS group. When compared to the control group, the DSS group displayed notable reductions of 40 and 57% in the expression levels of the CD163 and CD206 genes, respectively. However, there was no substantial increase in CD163 and CD206 gene expressions observed in the CCM-Co-ZIF-8 treatment group in comparison to the DSS group. These results indicate that the therapeutic potential of CCM-Co-ZIF-8 in addressing inflammation at the gene level primarily involves the suppression of proinflammatory factor expression.

After oral administration of CCM-Co-ZIF-8, as depicted in Figure 6b, a significant decrease in the expression level of CD68 was observed in the colon tissues, indicating that CCM-Co-ZIF-8 can inhibit the expression of proinflammatory factors.

https://doi.org/10.1021/acsomega.4c02446
ACS Omega 2024, 9, 30571−30582

4. CONCLUSIONS

In summary, Co-doped ZIF-8 was successfully synthesized by using a solution stirring method. The resulting material exhibited ROS-related enzyme (POD, CAT, and SOD) activities, enabling the elimination of reactive ROS. Furthermore, curcumin, an anti-inflammatory drug, was successfully loaded onto Co-ZIF-8 using room temperature by facile operation. The encapsulated drug CCM could be released in an acidic environment (pH = 5.5, inflammatory tissue). In vitro cell experiments demonstrated excellent cellular compatibility of CCM, Co-ZIF-8, and CCM-Co-ZIF-8. The investigation of anti-inflammatory properties revealed that CCM-Co-ZIF-8 primarily regulated macrophage polarization by reducing the expression of proinflammatory cytokines. Therefore, the experimental results demonstrate the potential application of CCM-Co-ZIF-8 for the treatment of colitis-associated inflammation.

■ ASSOCIATED CONTENT

Supporting Information

The supporting Information is available free of charge at https://pubs.acs.org/doi/10.1021/acsomega.4c02446.

Raman spectra of curcumin, Co-ZIF-8 and CCM-Co-ZIF-8; the particle size distribution of (a) Co-ZIF-8 and (b) CCM-Co-ZIF-8; blood biochemistryparametersof CCM-Co-ZIF-8 in mice; colon photos of mice with colitis treated with CCM-Co-ZIF-8; primer sequences for quantitative q-PCR; DAI scores are based on disease marker intens (PDF)

■ AUTHOR INFORMATION

Corresponding Authors

Hang Yao − *College of Chemistry and Chemical Engineering, Yangzhou University, Yangzhou 225002, P. R. China*; Email: yaohang@yzu.edu.cn

Dong-An Wang − *Department of Biomedical Engineering, City University of Hong Kong, Kowloon Tong 999077 Hong Kong SAR, P. R. China*; orcid.org/0000-0002-7927-1422; Email: dwang229@cityu.edu.hk

Hui Chong − *College of Chemistry and Chemical Engineering, Yangzhou University, Yangzhou 225002, P. R. China*; orcid.org/0000-0002-5847-3789; Email: chonghui@yzu.edu.cn

Authors

Qi Tao − *College of Chemistry and Chemical Engineering, Yangzhou University, Yangzhou 225002, P. R. China*

Feifei Wang − *College of Chemistry and Chemical Engineering, Yangzhou University, Yangzhou 225002, P. R. China*

Zehao Gu − *College of Chemistry and Chemical Engineering, Yangzhou University, Yangzhou 225002, P. R. China*

Xiaofei Yang − *College of Chemistry and Chemical Engineering, Yangzhou University, Yangzhou 225002, P. R. China*

Yuchi Zhao − *Department of Orthopedics, Yantaishan Hospital Affiliated to Binzhou Medical University, Yantai 264003, P. R. China*

Huan Pang − *College of Chemistry and Chemical Engineering, Yangzhou University, Yangzhou 225002, P. R. China*

Complete contact information is available at: https://pubs.acs.org/10.1021/acsomega.4c02446

Notes

The authors declare no competing financial interest.

■ ACKNOWLEDGMENTS

The authors acknowledge the Young Scientists Lifting Project of Jiangsu Province, China (TJ-2022-072), the Yantai Science and Technology Plan Project (2022MSGY072), the Graduate Student Innovation Foundation of Jiangsu Province (KYCX21_3202, Yangzhou University), and the Natural Science Foundation of Jiangsu Province (Grant BK20190903).

■ REFERENCES

(1) Katsanos, K. H.; Papadakis, K. A. Inflammatory Bowel Disease: Updates on Molecular Targets for Biologics. *Gut Liver* **2017**, *11* (4), 455−463.

(2) Kim, J. H.; Kim, J. W. [Effect of Immunomodulators and Biologic Agents on Malignancy in Patients with Inflammatory Bowel Disease]. *Korean J. Gastroenterol.* **2017**, *70* (4), 162−168.

(3) Roediger, W. E. W. Causation of human ulcerative colitis: A lead from an animal model that mirrors human disease. *JGH Open* **2019**, *3* (4), 277−280.

(4) Marchioni Beery, R.; Kane, S. Current approaches to the management of new-onset ulcerative colitis. *Clin. Exp. Gastroenterol.* **2014**, *7*, 111−132.

(5) Ferretti, F.; Cannatelli, R.; Monico, M. C.; Maconi, G.; Ardizzone, S. An Update on Current Pharmacotherapeutic Options for the Treatment of Ulcerative Colitis. *J. Clin Med.* **2022**, *11* (9), 2302 DOI: 10.3390/jcm11092302.

(6) Neurath, M. F. Current and emerging therapeutic targets for IBD. *Nat. Rev. Gastroenterol. Hepatol.* **2017**, *14* (5), 269−278.

(7) Macdonald, T. T.; Monteleone, G. Immunity, inflammation, and allergy in the gut. *Science* **2005**, *307* (5717), 1920−1925.

(8) Lei, P.; Yu, H.; Ma, J.; Du, J.; Fang, Y.; Yang, Q.; Zhang, K.; Luo, L.; Jin, L.; Wu, W.; Sun, D. Cell membrane nanomaterials composed of phospholipids and glycoproteins for drug delivery in inflammatory bowel disease: A review. *Int. J. Biol. Macromol.* **2023**, *249*, No. 126000.

(9) Xavier, R. J.; Podolsky, D. K. Unravelling the pathogenesis of inflammatory bowel disease. *Nature* **2007**, *448* (7152), 427−434. From NLM.

(10) Lin, Y.; Yang, X.; Yue, W.; Xu, X.; Li, B.; Zou, L.; He, R. Chemerin aggravates DSS-induced colitis by suppressing M2 macrophage polarization. *Cell Mol. Immunol.* **2014**, *11* (4), 355−366.

(11) Yang, Y.; Yang, L.; Jiang, S.; Yang, T.; Lan, J.; Lei, Y.; Tan, H.; Pan, K. HMGB1 mediates lipopolysaccharide-induced inflammation via interacting with GPX4 in colon cancer cells. *Cancer Cell Int.* **2020**, *20*, 205.

(12) Zhao, C.; Deng, H.; Chen, X. Harnessing immune response using reactive oxygen Species-Generating/Eliminating inorganic biomaterials for disease treatment. *Adv. Drug Delivery Rev.* **2022**, *188*, No. 114456.

(13) Oshitani, N.; Sawa, Y.; Hara, J.; Adachi, K.; Nakamura, S.; Matsumoto, T.; Arakawa, T.; Kuroki, T. Functional and phenotypical activation of leucocytes in inflamed human colonic mucosa. *J. Gastroenterol. Hepatol.* **1997**, *12* (12), 809−814, DOI: 10.1111/j.1440-1746.1997.tb00376.x.

(14) Wang, S.; Zhang, J.; Li, W.; Chen, D.; Tu, J.; Sun, C.; Du, Y. Hyaluronic acid-guided assembly of ceria nanozymes as plaque-targeting ROS scavengers for anti-atherosclerotic therapy. *Carbohydr. Polym.* **2022**, *296*, No. 119940.

(15) Zanconato, F.; Forcato, M.; Battilana, G.; Azzolin, L.; Quaranta, E.; Bodega, B.; Rosato, A.; Bicciato, S.; Cordenonsi, M.; Piccolo, S. Genome-wide association between YAP/TAZ/TEAD and AP-1 at enhancers drives oncogenic growth. *Nat. Cell Biol.* **2015**, *17* (9), 1218−1227.

(16) Ai, L.; Ren, Y.; Zhu, M.; Lu, S.; Qian, Y.; Chen, Z.; Xu, A. Synbindin restrains proinflammatory macrophage activation against microbiota and mucosal inflammation during colitis. *Gut* **2021**, *70* (12), 2261−2272.

(17) Li, Z.; Ma, D.; Wang, Y.; Wu, S.; Wang, L.; Jiang, Y.; Zhang, Y.; Li, X. Astragali Radix-Coptis Rhizoma Herb Pair Attenuates Atherosclerosis in ApoE−/− Mice by Regulating the M1/M2 and Th1/Th2 Immune Balance and Activating the STAT6 Signaling Pathway. *J. Evidence-Based Complementary Altern. Med.* **2022**, *2022*, No. 7421265, DOI: 10.1155/2022/7421265.
(18) Kattah, M. G.; Milush, J. M.; Burt, T.; McCabe, R. P., Jr.; Whang, M. I.; Ma, A.; Mahadevan, U. Anti-TNF and thiopurine therapy in pregnant IBD patients does not significantly alter a panel of B-cell and T-cell subsets in 1-year-old infants. *Clin. Transl. Gastroenterol.* **2018**, *9* (4), e143 DOI: 10.1038/s41424-018-0018-3.
(19) Lubschinski, T. L.; Pollo, L. A. E.; Mohr, E. T. B.; da Rosa, J. S.; Nardino, L. A.; Sandjo, L. P.; Biavatti, M. W.; Dalmarco, E. M. Effect of Aryl-Cyclohexanones and their Derivatives on Macrophage Polarization In Vitro. *Inflammation* **2022**, *45* (4), 1612−1630.
(20) Yao, H.; Wang, F.; Chong, H.; Wang, J.; Bai, Y.; Du, M.; Yuan, X.; Yang, X.; Wu, M.; Li, Y.; Pang, H. A Curcumin-Modified Coordination Polymers with ROS Scavenging and Macrophage Phenotype Regulating Properties for Efficient Ulcerative Colitis Treatment. *Adv. Sci.* **2023**, *10* (19), No. e2300601.
(21) Liu, J.; Liang, J.; Xue, J.; Liang, K. Metal-Organic Frameworks as a Versatile Materials Platform for Unlocking New Potentials in Biocatalysis. *Small* **2021**, *17* (32), No. e2100300.
(22) Sang, Y.; Cao, F.; Li, W.; Zhang, L.; You, Y.; Deng, Q.; Dong, K.; Ren, J.; Qu, X. Bioinspired Construction of a Nanozyme-Based H(2)O(2) Homeostasis Disruptor for Intensive Chemodynamic Therapy. *J. Am. Chem. Soc.* **2020**, *142* (11), 5177−5183.
(23) Wang, Z.; Zhang, Y.; Wang, X.; Han, L. Flow-homogeneous electrochemical sensing system based on 2D metal-organic framework nanozyme for successive microRNA assay. *Biosens. Bioelectron.* **2022**, *206*, No. 114120.
(24) Chen, J.; Huang, L.; Wang, Q.; Wu, W.; Zhang, H.; Fang, Y.; Dong, S. Bio-inspired nanozyme: a hydratase mimic in a zeolitic imidazolate framework. *Nanoscale* **2019**, *11* (13), 5960−5966.
(25) Nair, H. B.; Sung, B.; Yadav, V. R.; Kannappan, R.; Chaturvedi, M. M.; Aggarwal, B. B. Delivery of antiinflammatory nutraceuticals by nanoparticles for the prevention and treatment of cancer. *Biochem. Pharmacol.* **2010**, *80* (12), 1833−1843.
(26) Momtazi-Borojeni, A. A.; Abdollahi, E.; Nikfar, B.; Chaichian, S.; Ekhlasi-Hundrieser, M. Curcumin as a potential modulator of M1 and M2 macrophages: new insights in atherosclerosis therapy. *Heart Failure Rev.* **2019**, *24* (3), 399−409, DOI: 10.1007/s10741-018-09764-z.
(27) Tiwari, A.; Singh, A.; Garg, N.; Randhawa, J. K. Curcumin encapsulated zeolitic imidazolate frameworks as stimuli responsive drug delivery system and their interaction with biomimetic environment. *Sci. Rep.* **2017**, *7* (1), No. 12598.
(28) Zhou, S.; Su, Y.; Yang, X.; Liang, G.; Luo, S.; Song, X.; Situ, W. Different molecular structure of zeolite imidazole acid framework with curcumin loading and its antibacterial property. *Food Biosci.* **2023**, *54*, 102874 DOI: 10.1016/j.fbio.2023.102874.
(29) Jiang, B.; Duan, D.; Gao, L.; Zhou, M.; Fan, K.; Tang, Y.; Xi, J.; Bi, Y.; Tong, Z.; Gao, G. F.; et al. Standardized assays for determining the catalytic activity and kinetics of peroxidase-like nanozymes. *Nat. Protoc.* **2018**, *13* (7), 1506−1520.
(30) Liu, Y.; Zhang, Y.; Liu, Q.; Wang, Q.; Lin, A.; Luo, J.; Du, Y.; Lin, Y. W.; Wei, H. In vitro measurement of superoxide dismutase-like nanozyme activity: a comparative study. *Analyst* **2021**, *146* (6), 1872−1879.
(31) Delfini, M.; Stakenborg, N.; Viola, M. F.; Boeckxstaens, G. Macrophages in the gut: Masters in multitasking. *Immunity* **2022**, *55* (9), 1530−1548.
(32) Zhou, Y.; Ji, G.; Yang, X.; Chen, Z.; Zhou, L. Behavioral abnormalities in C57BL/6 mice with chronic ulcerative colitis induced by DSS. *BMC Gastroenterol.* **2023**, *23* (1), 84.
(33) Xu, L.; Liu, B.; Huang, L.; Li, Z.; Cheng, Y.; Tian, Y.; Pan, G.; Li, H.; Xu, Y.; Wu, W.; et al. Probiotic Consortia and Their Metabolites Ameliorate the Symptoms of Inflammatory Bowel Diseases in a Colitis Mouse Model. *Microbiol. Spectrum* **2022**, *10* (4), No. e00657-22, DOI: 10.1128/spectrum.00657-22.
(34) El-Guindy, D. M.; Elgarhy, L. H.; Elkholy, R. A.; Ali, D. A.; Helal, D. S. Potential role of tumor-associated macrophages and CD163/CD68 ratio in mycosis fungoides and Sézary syndrome in correlation with serum sCD163 and CCL22. *J. Cutaneous Pathol.* **2022**, *49* (3), 261−273, DOI: 10.1111/cup.14155.
(35) Ni, C.; Yang, L.; Xu, Q.; Yuan, H.; Wang, W.; Xia, W.; Gong, D.; Zhang, W.; Yu, K. CD68- and CD163-positive tumor infiltrating macrophages in non-metastatic breast cancer: a retrospective study and meta-analysis. *J. Cancer* **2019**, *10* (19), 4463−4472, DOI: 10.7150/jca.33914.

https://doi.org/10.1021/acsomega.4c02446
ACS Omega 2024, 9, 30571−30582